Modelling the Structure and Temporal Dynamics of the Moscow Surface Urban Heat Island Using Medium-Resolution Satellite Data

Oleg R. Malyuta[1*]

[1]National Research University Higher School of Economics (HSE), Faculty of Geography and Geoinformation Technologies, Moscow, Russia – ormalyuta@edu.hse.ru

Keywords: Urban heat island, Land surface temperature, Landsat, Local Climate Zones, Moscow, Remote sensing

Abstract

Urban heat island (UHI) amplification poses growing risks to public health and energy demand, yet long-term, city-scale diagnostics remain scarce for rapidly transforming metropolises. Here we present the first 40-year reconstruction of Moscow's surface UHI (SUHI) using 125 cloud-screened summer Landsat scenes (1984–2024, 30 m). Land surface temperature was retrieved with a single-channel algorithm constrained by MERRA-2 water vapor fields and emissivity from NDVI-based method; accuracy is ±2°C. SUHI intensity aggregated into annual and eight 5-year epochs. Eight Local Climate Zones (LCZs) were mapped from very high-resolution imagery and spectral indices to analyse morphology–temperature links.

The results show that the thermally significant SUHI footprint (> 2°C) expanded by 35 % (≈ 1040 km^2) and now covers just under 4000 km^2. Growth was highly uneven: New Moscow added 125 %, Old Moscow 19 %, and the suburban belt 35 %. LCZ trends reveal the fastest warming in new development (+0.19°C yr^{-1}) and industrial areas (+0.13°C yr^{-1}); forest and landscape parks warmed least (< 0.06°C yr^{-1}). Built-up index correlates strongly with mean LST (r = 0.68). Scenario mapping, informed by official land use plans, projects further intensification of SUHI along the Kaluzhskoye and Kievskoye highways and adjacent streets by 2035.

The openly available Google Earth Engine & Python implemented workflow is transferable to other cities, providing a template for climate-resilient planning and targeted green infrastructure interventions.

1. Introduction

Urban heat islands (UHI) represent a significant environmental challenge for modern cities, affecting public health, thermal comfort, energy demand, and local ecosystems (Oke, 1982). With global urbanization accelerating, understanding surface urban heat islands (SUHI) becomes crucial for sustainable urban planning and adaptation to climate change. Moscow, as Russia's largest metropolis, has undergone profound urban transformations since the 1990s, experiencing extensive suburbanization, industrial restructuring, and infill development. These processes have significantly altered its urban climate conditions, but detailed, long-term analyses of Moscow's SUHI evolution at medium spatial resolutions remain scarce. Previous SUHI studies in Moscow predominantly used low-resolution thermal imagery (e.g., MODIS at 1 km resolution) or relied on limited ground-based meteorological stations. Consequently, existing literature lacks detailed analyses of spatial and temporal SUHI dynamics at finer scales, limiting their practical applicability for urban climate analysis and planning.

To address this research gap, our study reconstructs the spatiotemporal dynamics of Moscow's SUHI over the past 40 years (1984–2024) using medium-resolution Landsat imagery. We specifically aim to (1) quantify long-term SUHI area changes across the metropolitan region; (2) examine surface temperature patterns within different Local Climate Zones (LCZs) actual for Moscow to identify which urban typologies have experienced the strongest warming; and (3) provide a scenario-based SUHI forecast up to 2035 based on official urban planning documents. The methodological framework developed in this study is made openly available and is readily transferable for analysing SUHI dynamics in other rapidly developing urban areas globally.

2. Main Body

2.1 Study Area and Background

Moscow is a mid-latitude metropolis that has expanded from around 1000 km^2 in 1984 to more than 2500 km^2 after the 2012 south-western annexation ("New Moscow"). The city is in a humid continental climate with warm summers (mean air temperature in July ≈ 20°C) and cold, of ten snow covered winters. Rapid economic transition after the 1990s triggered large-scale infill construction, brownfield redevelopment and greenfield housing estates. These processes reshaped the surface energy balance: impervious cover grew, while anthropogenic heat and traffic volumes rose, leading to the expansion and intensification of UHI (Zhou et al., 2018). Earlier UHI investigations relied on sparse weather stations or low-resolution composites; a fine-scale, multi-decadal SUHI chronology for Moscow has been lacking for a more detailed analysis of the spatial structure of the phenomenon.

2.2 Data Sets

Satellite imagery. 125 cloud-filtered summer Landsat Tier 1 Raw Scenes acquired between 1 June and 31 August in 1984–2024 were used. Landsat 5 TM supplies a single TIR band 6 (10.40–12.50 µm) for 1984–2012, whereas Landsat 8 TIRS provides two TIR bands 10 and 11 (10.6–11.19 and 11.5–12.51 µm) for 2013–2024. Band 10 was used for Landsat 8 due to the stray-light artifact affecting TIRS band 11. All scenes are distributed at 30 m pixel size after USGS resampling with Google Earth Engine (GEE) access provided. *Atmospheric data.* Column water vapor (WV) content at 50 km resolution was extracted from MERRA-2 reanalysis, time-matched (±1 h) to each Landsat overpass (Gelaro et al., 2017). Air temperature validation used CRU TS

* Corresponding author

v4.07 0.5° data (June–August means). Access to the dataset is also available through Google Earth Engine. (Harris et al., 2020).
Ancillary spatial data:

- Very high-resolution imagery (Maxar/Google Earth, 2019–2024) supported Local Climate Zone (LCZ) mapping.
- Official functional zoning maps for "Old Moscow" (target year 2025) and New Moscow (draft 2035) underpinned the scenario forecast (Genplan, 2010; MosLaw, 2017).

2.3 Methodology

2.3.1 Pre-processing and LST Retrieval

Level 1 digital numbers were converted to top of atmosphere radiance L_λ using sensor gains and offsets according to equations (USGS, 2019):

$$L_\lambda = M_L Q_{\text{cal}} + A_L \quad (1)$$

where L_λ is the top of atmosphere spectral radiance (mW cm^{-2} sr^{-1} μm^{-1}), Q_{cal} is the DN value of each pixel, and ML and AL are the multiplicative and additive scaling coefficients from the metadata. Clouds and cloud shadows were masked with the CFMASK quality band. Brightness temperature Tb of TM band 6 and TIRS band 10 was calculated via the inverse Planck function (USGS, 2019):

$$T_b = \frac{K_2}{\ln\left(\frac{K_1}{L_\lambda}+1\right)} \quad (2)$$

where Tb is the brightness temperature at the top of the atmosphere (K), and K_1 and K_2 are the sensor-specific calibration constants (mW cm^{-2} sr^{-1} μm^{-1} and K, respectively). Land surface temperature (LST) was subsequently retrieved with the single-channel algorithm (Jiménez-Muñoz & Sobrino, 2008; 2014). This method linearizes Planck's law and introduces empirical "atmospheric functions" that depend on column water vapor — the main absorber of thermal-infrared radiation in the atmosphere. Surface emissivity ϵ was estimated by the NDVI-Based Emissivity Method (NBEM; (Van de Griend, 1993)): pixels below the 10th NDVI maximum percentile adopt a bare soil emissivity of 0.97, those above the 90th NDVI maximum percentile adopt a full vegetation emissivity of 0.99, and intermediate values are linearly interpolated. Water vapor value used for calculation was retrieved from MERRA-2 reanalysis data. The atmospheric transmission C_{ij} coefficients used for the calculations were taken from the results of radiation modelling based on the atmosphere profiles of TIGR2311 (Landsat 5) and GAPRI4838 (Landsat 8) databases performed by (Jiménez-Muñoz & Sobrino, 2008; 2014). NDBI and the BU index were also calculated using processed images:

$$\text{NDBI} = \frac{\text{SWIR}+\text{NIR}}{\text{SWIR}-\text{NIR}} \quad (3)$$

$$\text{BU} = \text{NDBI} - \text{NDVI} \quad (4)$$

2.3.2 SUHI Derivation and Epoch Averaging

SUHI intensity is defined as

$$\text{SUHI} = LST_u - LST_r \quad (5)$$

where LST_u is the urban land surface temperature and LST_r is the rural surface temperature. Ten rural zones including villages, forests and arable lands were interpreted outside the Central Ring Road (CRR). LST data were normalized using rural mean LST value to retrieve SUHI intensity. To suppress weather-scale noise and reduce dimensionality, mean annual SUHI composites were averaged into eight five-year epochs mainly for visualizing purpose: 1984–88, 1989–93, 1994–1998, 1999–2003, 2004–2008, 2009–2014, 2015–2019 and 2020–24. No data were found for 1993, 1998, 2012 years. Considering 2°C algorithm's error (Jiménez-Muñoz & Sobrino, 2008), Pixels with SUHI > 2°C were classed as thermally significant.

2.3.3 Local Climate Zone Mapping

Following the Stewart and Oke LCZ conception (Stewart & Oke, 2012), eight LCZ classes relevant for Moscow were delineated by manual high-resolution imagery interpretation aided by NDVI, NDBI and SUHI data: industrial areas, squares, central areas, peripheral areas, new development areas, redevelopment areas, forest parks, landscape parks (Figure 1). A total of forty calibration polygons (3–8 per class) were produced for subsequent neighbourhood-level LST trend analysis.

2.3.4 LST Time-Series Analysis by LCZ

For samples of each LCZ class ordinary least-squares regression of annual mean LST was computed. To isolate intraurban variability from regional climate warming, class wise detrended values were also assessed (Figure 3). City mean summer LST was cross validated against summer CRU TS air temperature (Fig. 1) (Harris et al., 2020). The Wald test was used to test for statistical significance, and Durbin-Watson statistics calculated for autocorrelation test (values in range [1.5–2.5] are considered as negligible autocorrelation).

2.3.5 SUHI Area Time-Series by agglomeration parts

Long-term SUHI area (> 2°C) dynamics was summarized for three nested zones: Old Moscow (pre-2012 limits), New Moscow (annexed districts) and the Suburb belt between Moscow Ring Road and CRR excluding Moscow. Average annual SUHI area dynamics of selected zones between 1984 and 2024 were calculated to compare its expansion rates.

2.3.6 Scenario-Based Forecast (2035)

Actual Moscow master plan up to 2025 and New Moscow functional zones map up to 2035 were rasterized and harmonized into seven general functional categories: public, compact residential, dispersed residential, industrial, transport, natural, water. Median values and standard deviations of SUHI were calculated for Moscow's 2025 functional zones and transferred to the corresponding zones of New Moscow for 2035 producing an experimental outlook thermal map for the near future (Figure 4).

2.3.7 Processing Workflow

The complete Google Earth Engine processing code and accompanying Python analysis notebooks are openly available at `https://doi.org/10.5281/zenodo.17468921`.
They are fully documented in English and can be easily adapted for SUHI studies in any other region imaged by Landsat 5 & 8. These resources include:

- **Server-side (GEE) script** for image preprocessing, SUHI computation, epoch averaging, LST trend extraction by

LCZ, and zonal statistics for SUHI footprint calculation by part of ROI, providing a full SUHI investigation solution.

- **Client-side (Python) notebooks** for retrieved statistics analysis and visualizing.

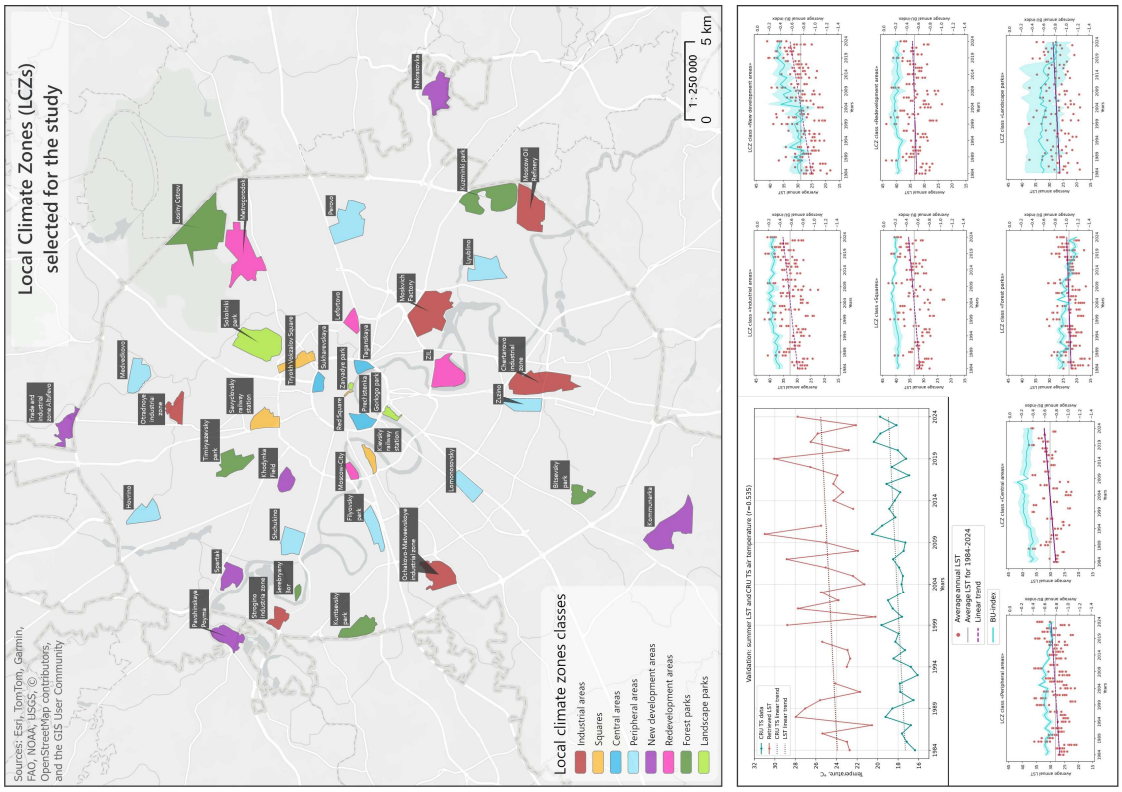

Figure 1. Selected LCZs in Moscow with associated annual surface temperature trends (1984–2024) by class and general LST data validation against CRU TS air temperature.

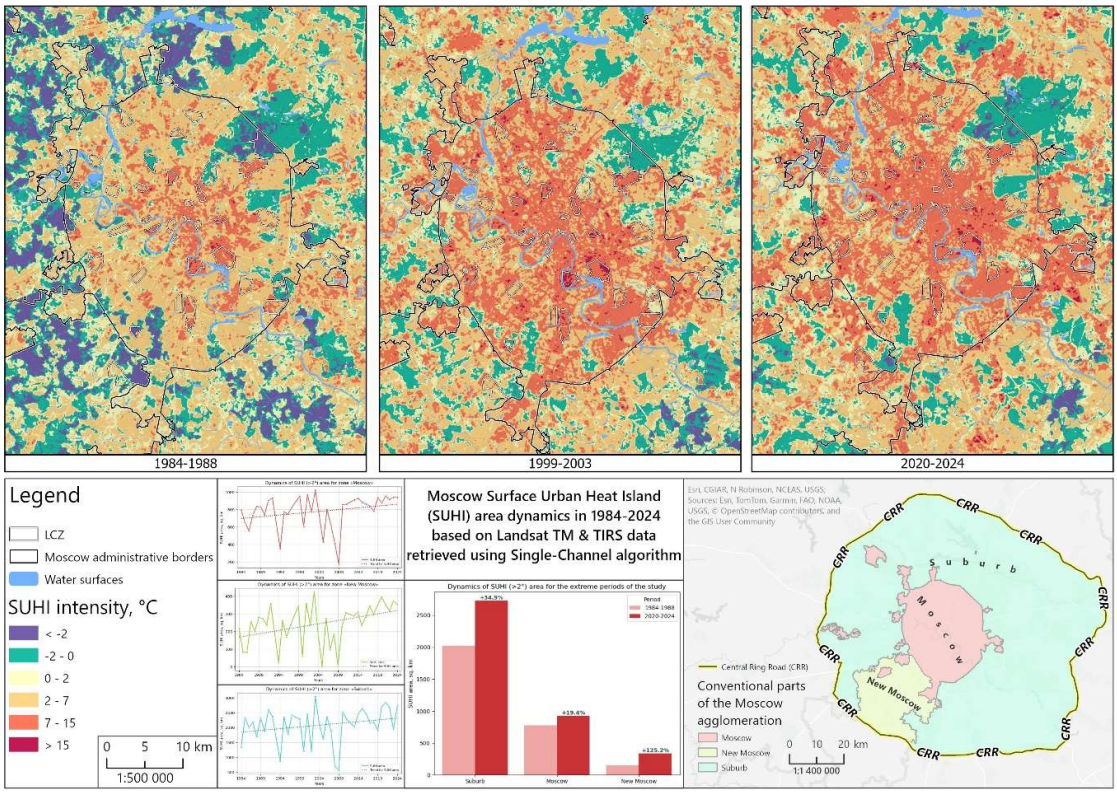

Figure 2. Five-year averaged Landsat-derived SUHI intensity maps for the Moscow agglomeration (1984–1988, 1999–2003, 2020–2024) with corresponding SUHI area dynamics for Suburb, Moscow, and New Moscow.

2.4 Results and Discussion

2.4.1 Validation with CRU TS

The city-averaged LST correlates moderately with the air temperature of the CRU TS (r = 0.53), and both records exhibit comparable warming slopes of approximately +0.04°C yr^{-1} (Table 1). The LST trend itself is not statistically significant (p = 0.24), largely because image availability, cloud cover, and weather anomalies introduce noise. Nevertheless, the close agreement of the two slopes supports the physical consistency of the LST retrieval and justifies its use for subsequent SUHI analysis.

Data set	Trend (°C yr^{-1})	p-value	Durbin-Watson
CRU TS	+0.04117	0.002	2.01
Computed LST	+0.04038	0.238	2.26

Table 1. City-averaged summer temperature trends (1984–2024).

2.4.2 Spatiotemporal Expansion of the Moscow SUHI Footprint

The thermally significant SUHI footprint (> 2°C) expanded from 2 944 km^2 in 1984–88 to 3 987 km^2 in 2020–24, a net gain of +35 % across the Moscow agglomeration. Growth was highly uneven: New Moscow recorded an explosive +125% increase (+187 km^2), Old Moscow added 150 km^2 (+19%), and the suburban belt gained 706 km^2 (+35 %); see Figure 2.
In Table 2 by comparing relative trends, it is clear that New Moscow SUHI expands 1.7 times faster than in Old Moscow and 2.9 times faster than in the Suburb.

Study site	Area (km^2)	Change rate ($km^2\ yr^{-1}$)	Rel. Change (yr^{-1})
Moscow	1115.14	+4.08	0.0037
New Moscow	614.74	+3.75	0.0061
Suburb	5736.51	+11.78	0.0021

Table 2. SUHI area average annual dynamic in 1984–2024 by agglomeration part.

Drivers and implications. The dominant driver of this expansion is the relentless conversion of vegetated or agricultural surfaces to impervious surfaces. In New Moscow, vast greenfield tracts were rapidly replaced by dense residential and commercial blocks built with low-albedo materials such as asphalt and concrete (e.g. "Kommunarka"). These surfaces absorb more solar energy, store sensible heat, and reradiate it at night, accounting for the more than two-fold increase in SUHI area. A similar pattern of new-development expansion occurs in the peripheral districts of Old Moscow, though in general it shows more moderate growth driven by infill and peripheral densification, while isolated brownfield redevelopments (e.g. “ZIL”, “Serp i Molot (Lefortovo)”, as well as new parks (e.g. "Zaryadye") demonstrate that strategic greening within mixed-use projects can locally dampen SUHI intensity (see Fig.1). This cooling effect of brownfield-to-green conversion has also been confirmed for the Moscow region by other studies (e.g. Lokoschenko et al., 2023).

2.4.3 Local Climate Zone Warming in Moscow

Linear trends extracted from study LCZ classes (1984–2024) reveal pronounced heterogeneity (Table 3 and Fig. 1). Detrended LST data (Fig. 3) show increasingly frequent positive anomalies after 2000 in the fastest-warming classes (Fig. 3 a–d).

Interpretation.

- **New development areas** warm fastest (+0.19°C yr^{-1}), reflecting recent construction on former croplands and grasslands.
- **Legacy industrial zones** follow at +0.13°C yr^{-1}, consistent with large impervious fractions and year-round anthropogenic heat.
- **Squares** and compact **central districts** gain +0.10°C yr^{-1} owing to low albedo and scarce tree canopy.
- **Peripheral residential areas** remain intermediate +0.07°C yr^{-1}, buffered by higher vegetation yet increasingly affected by infill.
- **Landscape** and **forest parks** warm slowest; trends are weak or insignificant, underscoring the cooling role of mature vegetation.
- **Redevelopment areas** exhibit the weakest (≤ +0.04°C yr^{-1}) insignificant trends demonstrating that brownfield conversion to mixed use plus greening can offset background warming.

Across all polygons the built-up (BU) index correlates strongly with mean LST (Pearson r = 0.68), reaffirming vegetation fraction as the primary modulator of intraurban thermal contrast.

2.4.4 Forecast Hot-Spots to 2035 for New Moscow

According to scenario maps derived from approved land use frameworks, by 2035 SUHI growth is projected to follow the principal southwest transport axes: Kaluzhskoye and Kievskoye highways, as well as the connecting Filatovskoye, Filimonkovskoye and Rakitki routes, engulfing settlements such as Troitsk, Ostafyevo and Vatutinki and others (Fig. 4). Integrating high-albedo materials, expansive street-tree programmes and blue-green infrastructure into these developments is therefore critical. Detailed appraisal of such measures, however, lies beyond the present scope.

2.4.5 Methodological Limitations and Future Work

Several factors constrain the accuracy and completeness of the present SUHI analysis:

1. **Single-channel retrieval uncertainty.** The algorithm incurs ±2°C error (Jiménez-Muñoz & Sobrino, 2008) under typical atmospheric conditions, propagating directly into SUHI intensity.
2. **Temporal gaps.** Cloud-free Landsat scenes are

missing for 1993, 1998 and 2012, so five-year epoch averaging masks some interannual variability.

LCZ class	Slope ($^{\circ}C\ yr^{-1}$)	p-value	Durbin-Watson
New development areas *(compact & open high-rise)*	**+0.19**	<0.01	1.7
Industrial areas *(heavy industry)*	**+0.13**	<0.01	2.27
Squares *(paved)*	+0.10	<0.01	2.11
Central areas *(compact mid-rise)*	+0.10	<0.01	2.18
Peripheral areas *(open mid- & high-rise)*	+0.07	<0.01	2.33
Landscape parks *(dense & scattered trees)*	+0.06	0.06	1.55
Forest parks *(dense trees)*	+0.04	0.02	2.20
Redevelopment areas *(varies)*	+0.04	0.17	1.90

Table 3. Linear warming trend by Local Climate Zone (1984–2024).
(Closest in meaning) LCZ from referenced classification (Stewart & Oke, 2012).

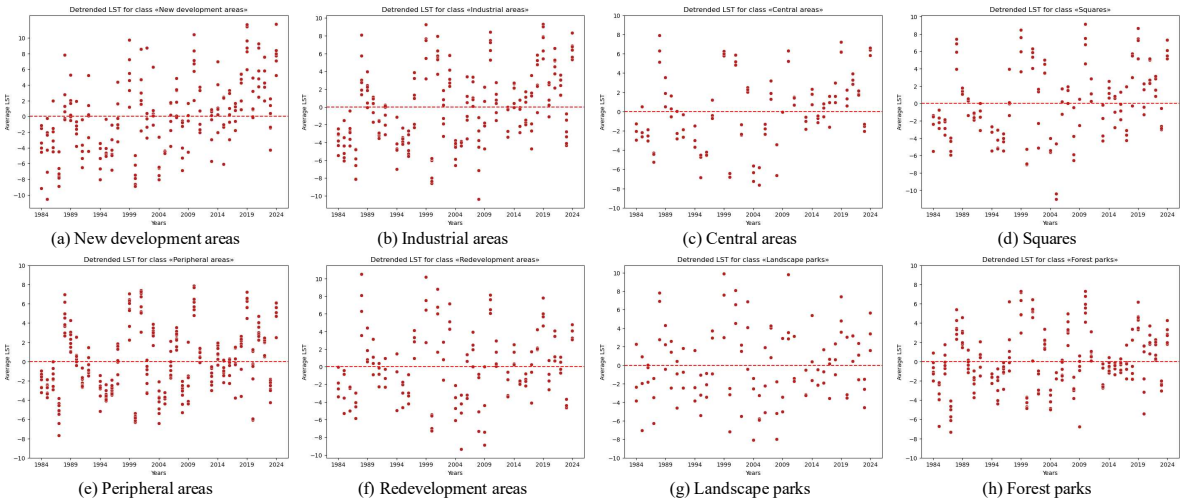

(a) New development areas (b) Industrial areas (c) Central areas (d) Squares

(e) Peripheral areas (f) Redevelopment areas (g) Landscape parks (h) Forest parks

Figure 3. Detrended LST anomalies for eight LCZ classes (1984–2024).

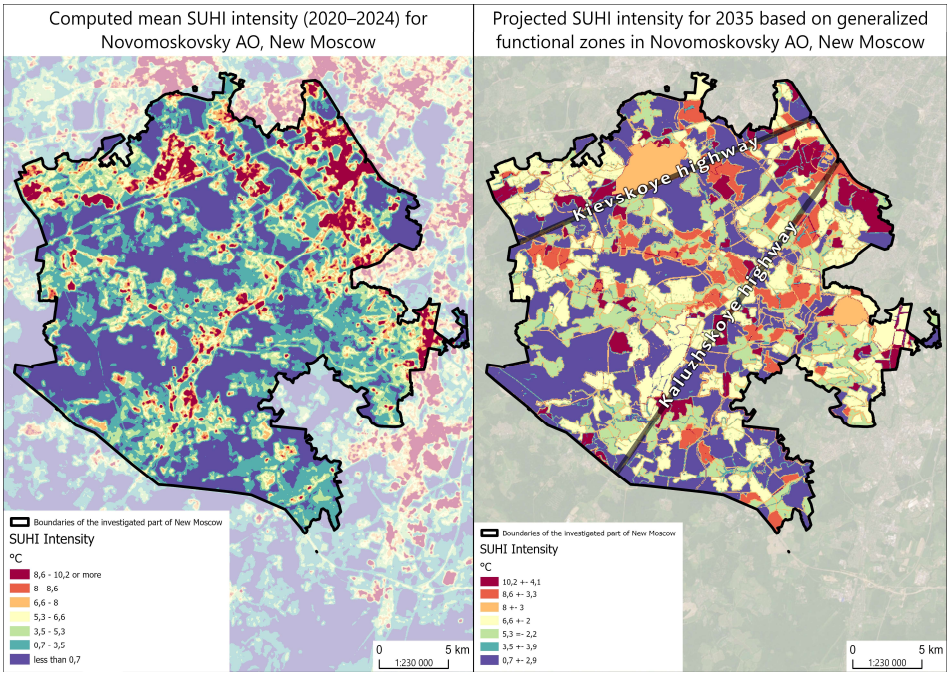

Figure 4. SUHI 2035 forecast for Novomoskovsky Administrative Okrug, New Moscow.

This contribution has been peer-reviewed. The double-blind peer-review was conducted on the basis of the full paper.
https://doi.org/10.5194/isprs-annals-X-4-W8-2025-487-2026 | © Author(s) 2026. CC BY 4.0 License.

3. **Coarse atmospheric data.** MERRA-2 provides water vapor columns at ~ 50 km resolution (Gelaro et al., 2017), yielding only two WV values across the study area and limiting spatial precision.

4. **Diurnal sampling bias.** Landsat overpasses (10 AM LT) precede the daily SUHI peak and cannot resolve sub-daily fluctuations.

Future work should test split-window LST retrieval, incorporate complementary night-time TIR observations, and evaluate mitigation scenarios via urban climate modelling. In addition, targeted research is needed to identify the optimal design parameters (e.g. size, shape and spacing) of green (parks, street trees) and blue (ponds, water features) infrastructure, as well as to explore alternative intervention strategies — such as high-albedo pavements, green roofs, and reflective coatings — for maximally effective SUHI attenuation.

3. Conclusions

This study presents the first 40-year intraurban investigation of Moscow's surface urban heat island (SUHI) using Landsat 5 & 8 thermal imagery. Over the past four decades, the SUHI footprint in the Moscow agglomeration has grown by 35%, with New Moscow seeing the most rapid SUHI area growth rates (+125%). Warming rates vary markedly by urban form, with new residential developments heating most rapidly (0.19°C yr^{-1}), followed by industrial zones (0.13°C yr^{-1}) and central districts (0.10°C yr^{-1}). Strategic redevelopment of brownfields and expansion of urban greenery can effectively curb further SUHI intensification and spatial spread. A 10-year outlook for New Moscow suggests continued SUHI advancement along key transport corridors (Kaluzhskoye and Kievskoye highways) and adjacent streets. Deploying targeted green infrastructure measures emerges as a critical adaptation strategy to mitigate heat island effects in newly built-up areas. The complete SUHI data retrieval & analysis workflow is publicly available at `https://doi.org/10.5281/zenodo.17468921` for application to any region. These findings can directly inform climate-resilient urban planning and heat risk management in rapidly developing cities.

Acknowledgements

The author is grateful to N.O. Telnova, senior lecturer at the National Research University Higher School of Economics for invaluable guidance and support throughout this study. Thanks are also due to the USGS for providing open access to the Landsat archive and to the Google Earth Engine team for their freely available processing platform.

References

Gelaro, R., McCarty, W., Suárez, M.J., Todling, R., Molod, A., Takacs, L., Randles, C.A., Darmenov, A., Bosilovich, M.G., Reichle, R., Wargan, K., Coy, L., Cullather, R., Draper, C., Akella, S., Buchard, V., Conaty, A., da Silva, A.M., Gu, W., Kim, G.K., Koster, R., Lucchesi, R., Merkova, D., Nielsen, J.E., Partyka, G., Pawson, S., Putman, W., Rienecker, M., Schubert, S.D., Sienkiewicz, M., Zhao, B., 2017. The Modern-Era Retrospective Analysis for Research and Applications, Version 2 (MERRA-2). *J. Climate*, 30(14), 5419–5454.

Harris, I., Osborn, T.J., Jones, P., Lister, D., 2020. Version 4 of the CRU TS monthly high-resolution gridded multivariate climate dataset. *Sci. Data*, 7, 109.

Jiménez-Muñoz, J.C., Sobrino, J.A., 2008. Revision of the single-channel algorithm for land surface temperature retrieval from Landsat thermal data. *IEEE Trans. Geosci. Remote Sens.*, 47(1), 339–349.

Jiménez-Muñoz, J.C., Sobrino, J.A., 2014. Land surface temperature retrieval methods from Landsat-8 thermal infrared sensor data. *IEEE Geosci. Remote Sens. Lett.*, 11(10), 1840–1843.

Lokoschenko, M.A., et al., 2023. Recent changes of the Moscow heat island. *Dokl. Earth Sci.*, 511(2), 243–253.

Moscow City Law No. 10 of 15 March 2017. On Amendments to the Moscow City Law No. 17 of 5 May 2010 "On the Master Plan of Moscow City". *Moscow City Legislation Collection*, 2017.

Moscow Master Plan 2025. Supplement to Moscow City Law "On the Master Plan of Moscow City" (Book 2: Maps and Territorial Planning Schemes). *Moscow City Architecture Committee,* Moscow, 2010.

Oke, T.R., 1982. The energetic basis of the urban heat island. *Q. J. R. Meteorol. Soc.*, 108(455), 1–24.

Stewart, I.D., Oke, T.R., 2012. Local climate zones for urban temperature studies. *Bull. Am. Meteorol. Soc.*, 93(12), 1879–1900.

USGS, 2019. Landsat 8 Surface Reflectance Product L2 User's Handbook, Version 2.0. *U.S. Geological Survey*, Sioux Falls, SD, USA.

Van de Griend, A.A., Owe, M., 1993. On the relationship between thermal emissivity and the normalized difference vegetation index for natural surfaces. *Int. J. Remote Sens.*, 14(6), 1119–1131.

Zhou, D., Xiao, J., Bonafoni, S., Berger, C., Deilami, K., Zhou, Y., Frolking, S., Yao, R., Qiao, Z., Sobrino, J.A., 2018. Satellite remote sensing of surface urban heat islands: Progress and perspectives. *Remote Sens.*, 11(1), 48.